Catalysis Science & Technology

ROYAL SOCIETY OF CHEMISTRY

PAPER

Cite this: *Catal. Sci. Technol.*, 2022, **12**, 3474

The critical role of Asp206 stabilizing residues on the catalytic mechanism of the *Ideonella sakaiensis* PETase†

Rita P. Magalhães, [ab] Henrique S. Fernandes [ab] and Sérgio F. Sousa *[ab]

Received 15th December 2021,
Accepted 18th March 2022

DOI: 10.1039/d1cy02271g

rsc.li/catalysis

Plastic accumulation is one of the main environmental issues of our time. In 2016, two enzymes capable of degrading polyethylene terephthalate (PET), one of the most common plastic polymers, were discovered. PETase and MHETase from *Ideonella sakaiensis* (*Is*PETase and *Is*MHETase, respectively) work sequentially to degrade PET to its constituent monomers. PETase catalyzes the cleavage of PET repetitive units ((mono-(2-hydroxyethyl)terephthalic acid (MHET)), whereas MHETase hydrolyses MHET into terephthalic acid (TPA) and ethylene glycol (EG). In this work, the catalytic mechanism of *Is*PETase was studied by QM/MM. The reaction was found to progress in four distinct steps, divided into two major events: formation of the first transition intermediate and hydrolysis of the adduct. The transition state and respective reactant and product of each step were fully characterized and described. The rate-limiting step was found to be step 3, with an activation barrier of 12.5 kcal mol^{-1}. Furthermore, in this study, we have shown the critical role of a triad of residues composed by Ser207, Ile208, and Ala209 in stabilizing the catalytic Asp206 residue. This finding confirms the importance of using a larger QM region since our results disclose some important differences when compared with previous computational studies of the same mechanism. These results provide valuable insights into the catalytic mechanism of *Is*PETase that can contribute to the rational development of more efficient engineered enzymes.

Introduction

Plastics are highly resistant long-chain polymers derived from fossil-fuel.[1] Since the beginning of massive plastic production in 1950,[2] these materials have become abundant and essential in everyday life globally.[3] The features that make plastics ideal materials – high durability, light weight, and low production cost[4] – are also responsible for their hazardous permanence in the environment.[4,5] Due to the lack of proper disposal and recycling strategies, plastics have accumulated and infiltrated terrestrial and marine settings, with harsh consequences for the environment, and human and animal health. One of the most produced single-use plastic polymers worldwide is polyethylene terephthalate (PET) (Fig. 1). PET is a long-chain polymer made up of repeating units of terephthalic acid (TPA) and ethylene glycol (EG) synthesized from polycondensation of TPA and EG (Fig. 1) or bis(2-hydroxyethyl)terephthalic acid (BHET) (Fig. 1).[6]

Recently, the usage of microorganism-produced enzymes for depolymerization and biodegradation of plastic materials, mainly PET, has become popular.[7–9] *Thermomonospora fusca* hydrolase (*Tf*H), the first enzyme capable of degrading PET, was identified in 2005.[10] Since

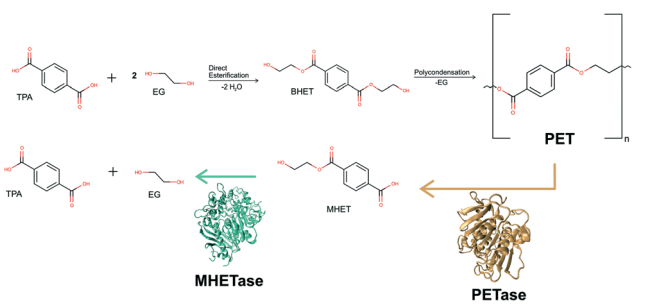

Fig. 1 Summary of PET synthesis and full enzymatic degradation by *Is*PETase and *Is*MHETase.

[a] *UCIBIO – Applied Molecular Biosciences Unit, BioSIM – Departamento de Biomedicina, Faculdade de Medicina, Universidade do Porto, 4200-319 Porto, Portugal. E-mail: sergiofsousa@med.up.pt*

[b] *Associate Laboratory i4HB – Institute for Health and Bioeconomy, Faculdade de Medicina, Universidade do Porto, 4200-319 Porto, Portugal*

† Electronic supplementary information (ESI) available: Molecular structures for reactant, transition state, and product of all steps of the mechanism (PDB files in a ZIP package); supplementary figures and tables (PDF); MD simulation (mov). See DOI: **https://doi.org/10.1039/d1cy02271g**

then, numerous enzymes have been discovered, isolated, characterized and described.[11–16] In 2016, a bacterium capable of using PET as its major energy and carbon source was discovered in a Japanese landfill.[17] *Ideonella sakaiensis*, the identified bacteria, secretes two enzymes responsible for PET degradation – *Is*PETase and *Is*MHETase. *Is*PETase depolymerizes PET to its composing MHET units (Fig. 1), and *Is*MHETase completes the degradation of MHET to TPA and EG (Fig. 1).[17]

Since initial reports verified high activity and specificity against PET polymer, *Is*PETase has received a lot of attention, and many structural and activity studies have been reported to date.[18–27] The enzyme assumes a canonical α/β-hydrolase fold with nine mixed β-strands that make up a central β-sheet, surrounded by seven α-helixes.[19] The presently accepted mechanistic proposal follows the typical serine hydrolase mechanism, fulfilled by a Ser–His–Asp (Ser160–His237–Asp206)[19] catalytic triad in the stabilizing presence of a two-residue oxyanion hole made up by the backbone of residues Tyr87 and Met161.[19] Several engineering studies have replaced these residues with alanine, and have evaluated the impact in the reaction with various PET-related substrates under different conditions, as described in Table 1. These changes resulted in a complete loss of activity for the modified catalytic triad residues and diminished activity in the variants affecting oxyanion hole residues.

Kinetic studies with PET substrate or analogues are scarce. Yoshida *et al.*[17] reported an approximate k_{cat} of 0.7 s^{-1} at 30 °C for BHET, whereas Ma *et al.*[28] have reported a k_{cat} of 27.0 s^{-1} at 30 °C for *para*-nitrophenyl acetate, corresponding to an activation Gibbs free energy of about 18.0 and 15.8 kcal mol^{-1}, respectively.

Quantum mechanics (QM) is the only computational methodology that allows the description of chemical reactions with an accuracy and predictability comparable with the experimental evidence. Unfortunately, the current computational resources and available algorithms cannot tackle biomolecular systems with the dimension of thousands of atoms, such as enzymes. Therefore, hybrid QM/MM simulations were developed, and awarded the Nobel Prize in Chemistry in 2013, to address these systems. In such methodology, the region of the system where the reaction took place, usually the active site, is treated using a high theoretical level (QM). The remaining system is treated using the computationally affordable molecular mechanics (MM) method, which allows a fast and reasonable description of geometry and electrostatic environment.

QM/MM studies have proved to have excellent outcomes in the accurate description of enzymatic mechanisms with extensive detail and unique reasoning for experimental data, such as structural, kinetic, and spectroscopic results. There have been reported many works where these QM/MM methods were successfully applied in the study of catalytic mechanisms of various enzymatic families such as proteases,[29,30] synthases,[31–33] hydrolases[34] and reductases.[35,36]

Among those QM/MM studies, several proposals regarding the general mechanism of *Is*PETase have been described in the literature.[18,19,37–39] However, some aspects have remained unexplained or subject to debate at the atomic level,[18,19,40] particularly concerning the number of steps involved in the mechanism and the active role of Asp206 residue. With respect to the number of steps, the computational studies of Boneta *et al.*[41] and Feng *et al.*[42] have shown that the reaction occurred in four sequential steps whereas Jerves *et al.*[43] reported a two-steps mechanism. Regarding the role of Asp206, its basic character was not observed in all studies, since some studies have reported the proton transfer from His237 to Asp206 (ref. 42) and other have proposed that the proton is not transferred and the Asp206 residue only stabilized the positively charged His237 formed during the reaction.[41,43]

A detailed QM/MM atomistic description of the catalytic mechanism of this enzyme, dissecting the role played by the different active-site amino acid residues, particularly the Asp206, and by the electronic distribution and charge effects at the transition state would provide valuable insights on bioengineering strategies for increasing their enzymatic efficiency for plastic degradation through rational enzyme mutagenesis.

Methodology

Structure preparation

This study was performed using the crystallographic structure of *Is*PETase from *Ideonella sakaiensis* deposited in the Protein

Table 1 Alanine mutations on catalytically relevant residues and the consequent effects

Mutated residues	Substrate	Conditions	Effect	Ref.
S160A/D206A/H237A	BHET	pH = 7.0 T = 30 °C	Complete loss of activity	19
	PET film	pH = 9.0 T = 30 °C		
	BHET	pH = 7.5 T = 30 °C		22
	PET bottle	pH = 9.0 T = 30 °C		
Y87A	BHET	pH = 7.0 T = 30 °C	5% of WT activity	19
	PET film	pH = 9.0 T = 30 °C	Lower MHET and TPA production[a]	
M161A	BHET	pH = 7.0 T = 30 °C	52% WT activity	
	PET film	pH = 9.0 T = 30 °C	Lower MHET and TPA production[a]	

[a] Production increases with time, indicating a kinetic alteration.[19]

Data Bank (PDB)[44] with the code 6EQE.[21] This structure was solved with a resolution of 0.92 Å and includes the complete sequence of *Is*PETase. Since structure 6EQE was in apo-form, 1-(2-hydroxyethyl)4-methyl terephthalate (HEMT), a model of PET substrate represented in Fig. 2, was obtained from PDB structure 5XH3 (ref. 18) and introduced in structure 6EQE after structural alignment with PyMOL software,[45] as shown in Fig. S2.†

Structure minimization and molecular dynamics

The protein–substrate complex was prepared with *pdb4amber* command from Amber18 (ref. 46) software package and protonated according to PlayMolecule ProteinPrepare server.[47] At physiological pH (7.0), two histidine residues were protonated at the δ-nitrogen, including catalytic histidine (His237) and His104. This protonation is in accordance with previous catalytic studies on this enzyme.[41–43] The full protonation server output is available in Table S1.† The MM parameters for HEMT were assigned using ANTECHAMBER considering GAFF, with RESP charges calculated at HF/6-31G(d) with Gaussian09.[48] The ff14SB force field was used for the subsequent simulations.[49] Six Cl^- ions were added in order to neutralize the system, which was immersed in a periodic box of TIP3P (ref. 50 and 51) water molecules extending 12 Å from solute. Geometry of the protein–ligand system was minimized through four sequential stages using the AMBER18 (ref. 46) software package. After two equilibration cycles, the system undergone a molecular dynamics (MD) simulation for 100 ns in an NPT ensemble at a temperature of 310.15 K and a pressure of 1.0 bar, considering a 2 fs integration step with periodic boundary conditions. Cut-off value for short-range interactions was set to 10.0 Å, and all bonds involving hydrogen atoms were constrained with SHAKE algorithm.[52] MD trajectory analysis was conducted using the cpptraj tool[53] and VMD software.[54] Full methodology details and protocol can be found in ESI.†

QM/MM

After MD trajectory analysis with cpptraj tool[53] and VMD software,[54] the structure with the minimum critical catalytic distances (Table 2) from the equilibrated portion of the production stage (Fig. S1†) was used to build the QM/MM model, using the molUP plugin,[55] available through the VMD Store[56] for VMD.[54]

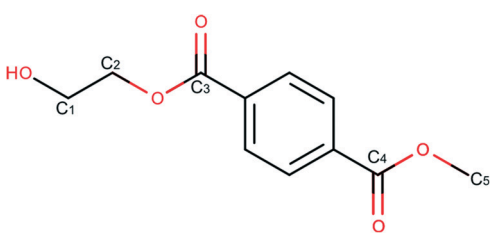

Fig. 2 HEMT structure.

Table 2 Relevant distances between residues included in the QM layer, following the notation in Fig. 4

1st residue	2nd residue	Distance (Å)
Ser160:OG	HEMT:C1	2.59
Ser160:HG	His237:NE2	1.68
His237:HD1	Asp206:OD2	1.68
Asp206:OD2	Ala209:H	1.94
Asp206:OD1	Ser207:H	2.24
	Ile208:H	1.94
	WAT:H	1.87
HEMT:O1	Tyr87:H	1.88
	Met161:H	2.17

The QM/MM model included the full protein–substrate complex and a 10.0 Å coating of water molecules.

The subtractive ONIOM QM/MM methodology[57] was used to address the catalytic mechanism of *Is*PETase. The system was divided into two regions: the catalytic region, treated at the quantum mechanical (QM) level, and a larger surrounding region, treated with molecular mechanics (MM), as evidenced by Fig. 3. The QM region was calculated with density functional theory (DFT).

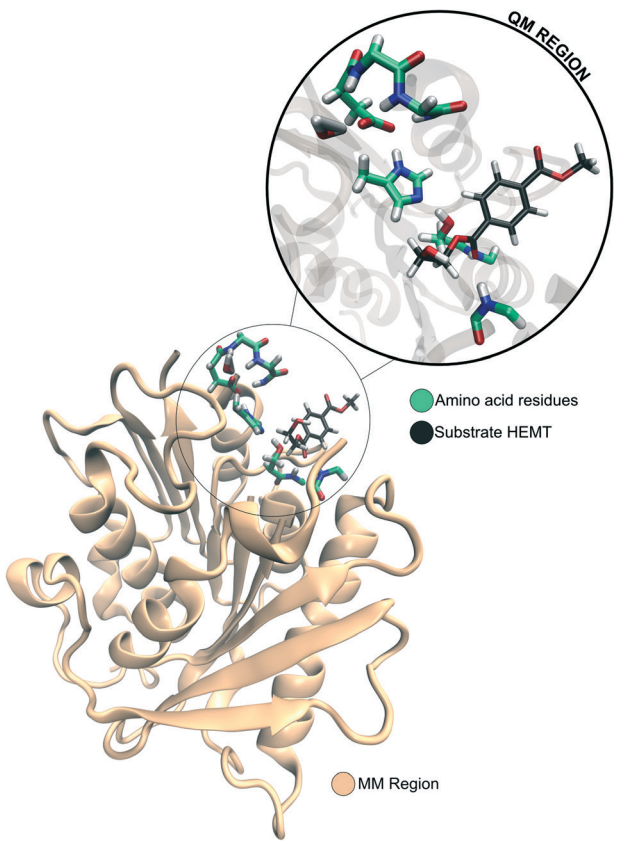

Fig. 3 QM/MM model employed in this study. The MM region is represented in new cartoon (orange), whilst the QM region is represented in licorice. The protein residues are in green and the substrate, HEMT, in black.

Regarding the interaction between the two ONIOM model layers, the electrostatic embedding method was used to perform all calculations.

Three models were built with different atoms included in the QM region, represented in Fig. 4. The respective relevant distances are described in Table 2. A 3D representation of the expanded QM region (model 3) can be found in Fig. S3.†

The initial model, model 1, included in the QM treated region atoms from the catalytic triad residues (Ser160, Asp206, and His237), the residues involved in the stabilization of the oxyanion hole (Met161 and Tyr87) and substrate analogue HEMT, amounting to a total of 64 atoms. Model 2 included, in addition to the amino-acid residues mentioned, residues Ser207, Ile208, and Ala209, and a water molecule that closely interacts with the Asp206, amounting to a total of 85 atoms. Subsequently, model 3 was built by the addition of Trp185 (total of 103 atoms) and is the main model discussed in this work. For all models, an additional water molecule was included in the QM region for the hydrolysis stage of the mechanism.

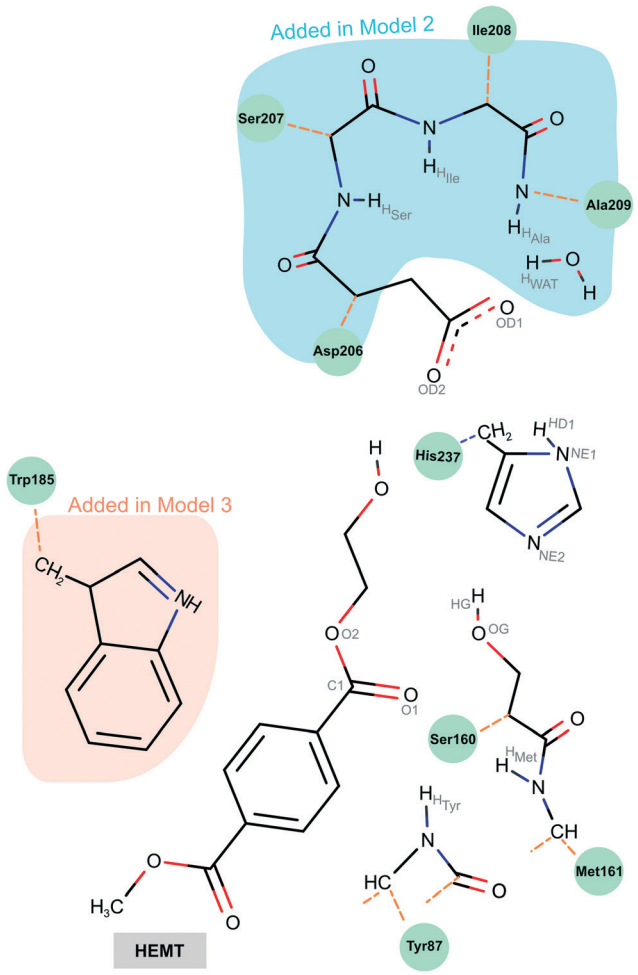

Fig. 4 Atoms included in the QM region in model 1 (white background, 64 atoms); model 2 (white and blue backgrounds, 85 atoms) and model 3 (white, blue, and orange background, 103 atoms). All covalent bonds spinning across QM/MM layers are represented by dashed orange lines. Amino acid residues are identified by the green labels, while the substrate (HEMT) is identified by a grey square.

Geometry optimization of the QM region was performed with the B3LYP[58–60] functional (DFT) and the 6-31G(d,p) basis set.[48] Linear scans along specific reaction coordinates in each step allowed for the exploration of the reactional space. From the higher energy structures of each scan, transition states (TS) candidate structures were obtained and optimized. Then, the structures of reactant and product were determined through internal reaction coordinate (IRC) calculations.[61] Confirmation of TSs and minima were done using vibrational frequency calculations. A single imaginary frequency was observed for the TSs associated with the vibration of the atoms involved in each step. Zero-point energy (ZPE) thermal and entropic corrections were estimated at 1.0 bar and 298.15 K during frequency calculations.

The electrostatic impact of different residues surrounding the QM region was assessed through single-point (SP) energy calculations with null charges for each individual residue up to 5 Å from the QM region.

The final electronic energies were refined through SP energy calculations using DLPNO-CCSD(T)/CBS.[62] These calculations were performed after isolation of the QM region with the ORCA software (v4.2.1).[63] SP energy calculations were performed for the isolated QM regions with B3LYP/6-31G(d,p) and DLPNO-CCSD(T) with the cc-pVDZ and cc-pVTZ basis sets, and the cc-pVDZ/C and cc-pVTZ/C correlation fitting basis sets, respectively. The combination of the energies obtained with the cc-pVDZ|cc-pVDZ/C and cc-pVTZ|cc-pVTZ/C basis sets for the QM region were used to extrapolate to the complete basis set (CBS) according to the ORCA implementation. The energy difference between the DLPNO-CCSD(T)/CBS and B3LYP/6-31G(d,p) were summed to the ONIOM energy obtained from geometry optimizations. This general approach has been used with success in the detailed atomic-level study of the catalytic mechanism of several enzymes.[64–69]

Activation and reaction Gibbs free energies for each reaction step were determined by the difference between the Gibbs free energies of TS and reactant, or product and reactant, respectively.

All the preparation of the Gaussian 09 (ref. 70) input files and result analysis was done using molUP plugin,[55] installed through VMD Store[56] for VMD software.[54]

Results and discussion

The catalytic mechanism of *Is*PETase

The catalytic mechanism of *Is*PETase was studied, in this work, considering primarily the extended QM region represented by model 3. In this section, all results refer to this model, and all geometry optimization calculations were performed considering the QM region of model 3. To make figures clearer, the following figures do not represent all atoms included in the QM region, since they are extensively represented in Fig. 4. A schematic description of the

mechanism with the entire QM region can be found in Fig. S12 and S13.† According to our results, the reaction follows a two-stages mechanism: 1) acylation and 2) deacylation. First, the formation of the acyl intermediate (Fig. 5) that occurs in two sequential steps. Then, the hydrolysis of the adduct (Fig. 6) also takes two steps.

Acylation mechanism

The first step involves the formation of the first tetrahedral intermediate (Fig. 5 – step 1). The reaction begins with the nucleophilic attack of the Ser160 OG oxygen to the C1 carbon of the substrate's ester bond. The reaction coordinate was the incremental decrease of the distance between the Ser160:OG and HEMT:C1 atoms. The charge-relay system between the Asp206 and His237 allows catalytic histidine to act as a base that enhances the nucleophile character of Ser160 residue. Upon attack by the Ser160, the charge in the substrate ester bond is delocalized to O1 atom and stabilized by an oxyanion hole made up by residues Met161 and Tyr87, as shown by the atomic distances between the residues (Met161:O1: 1.88 Å for the reactant *versus* 1.72 Å for the product; Tyr87:O1: 2.17 Å for the reactant *versus* 1.84 Å for the product).

Therefore, according to our calculations, the first step happens in a concerted manner. Proton HD1 remains bound to His237 throughout the reaction (HD1:NE1: 1.05 Å in the reactant *versus* 1.11 Å in the product) and makes a hydrogen bond with Asp206 (HD1:OD2: 1.68 Å in the reactant *versus* 1.45 Å in the product). Our data agree with the recently published works by Boneta *et al.*[41] and Jerves *et al.*,[43] where the HD1 proton is not transferred to the Asp206 in step 1. However, Feng *et al.*[42] have suggested that this proton

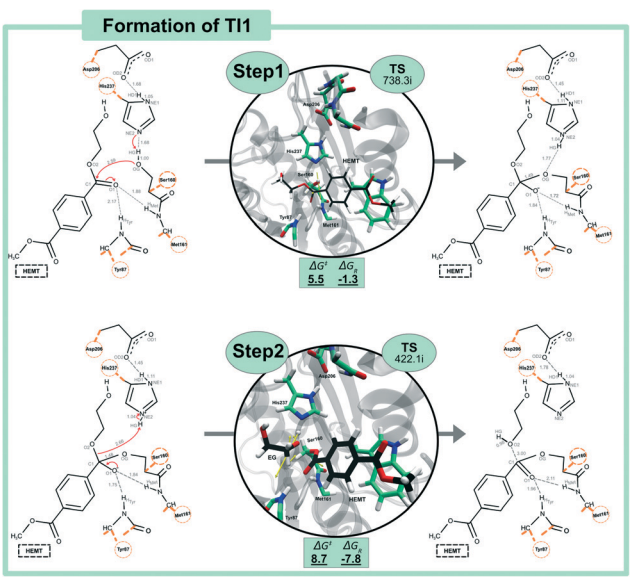

Fig. 5 Formation of the tetrahedral intermediate, comprising steps 1 and 2 of *Is*PETase calculated mechanism. The activation ($\Delta G^{\ddagger}$) and reaction (ΔG_R) Gibbs free energies are in kcal mol^{-1} and the single imaginary TS frequencies in cm^{-1}.

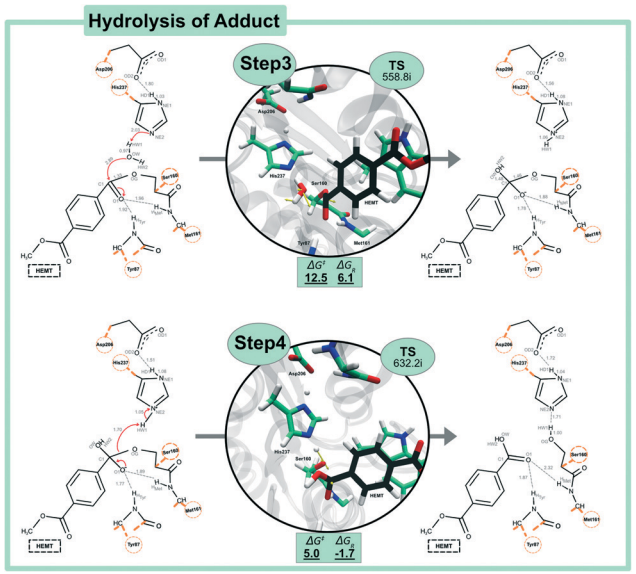

Fig. 6 Water-molecule mediated hydrolysis of the adduct, comprising steps 3 and 4 of *Is*PETase calculated mechanism. The activation ($\Delta G^{\ddagger}$) and reaction (ΔG_R) Gibbs free energies are in kcal mol^{-1} and the single imaginary TS frequencies in cm^{-1}.

transfer could occur 45% of the time, indicating a statistical possibility for both cases. The Feng *et al.*[42] results were obtained from a smaller QM region where Ser207, Ile208, and Ala209 residues were not included. According to our calculations, these three residues are crucial for the stabilization of Asp206, since we have observed the proton transfer when Ser207, Ile208, and Ala209 residues were not included in the QM region (model 1) (Fig. S11†). Our calculations show the importance of choosing the atoms and residues included in the QM region carefully to better describe catalytic mechanisms using hybrid QM/MM approaches, as previously highlighted.[71] Moreover, our calculations emphasize the role of single-point energy calculations with MM null charges residues to evaluate their impact on the estimated Gibbs free energies.

Abstraction of proton HG from Ser160 by His237 is confirmed by the distance of 1.04 Å between the proton and His237 NE2 atom in the reaction product, compared with 1.77 Å between HG and Ser160. At this point, His237 is double protonated with protons HG (originally from Ser160) and HD1, which remains bound to it. The TS was determined with an imaginary frequency at 738.3i cm^{-1}. Step 1 culminates in the formation of the first tetrahedral intermediate (Ser160/OG:HEMT/C1: 1.49 Å) with an activation Gibbs free energy of 5.5 kcal mol^{-1} and a reaction free energy of −1.3 kcal mol^{-1}.

The second step is the cleavage of the C1–O2 bond in the first tetrahedral intermediate, by abstraction of the His237 HG proton (O2:HG – 0.98 Å), yielding the first leaving product (Fig. 5 – step 2). The reaction coordinate followed in this step was an incremental increase in the distance between atoms C1 and O2 in the HEMT molecule. According to our simulations, this reaction occurs with an activation Gibbs

free energy of 8.7 kcal mol^{-1} and a reaction Gibbs free energy of −7.8 kcal mol^{-1}. The TS is characterized by an imaginary frequency at 422.1i cm^{-1}. At the end of step 2, an EG molecule is released and the remaining part of the HEMT molecule keeps covalently bound to Ser160, as confirmed by the 100 ns MD simulation of this structure in ESI.† Furthermore, rapid release of EG is shown by Fig. S4,† which represents the distance between the EG product and the HEMT molecule. The reaction proceeds through hydrolysis that requires the recruitment of a water molecule. Due to the highly exposed active site of *Is*PETase, a water molecule easily diffuses to the proximity of the HEMT-enzyme adduct, as shown by Fig. S5,† representing the radial distribution function (RDF) and the cumulative number of water molecules registered in the MD simulation of this structure.

According to our simulations, the acylation occurs through two sequential steps in an exergonic process (ΔG_R = −9.1 kcal mol^{-1}) with a maximum activation barrier of 8.7 kcal mol^{-1}.

Deacylation mechanism

The hydrolysis stage, comprising steps 3 and 4, begins with the abstraction of a water molecule proton (HW1) by the NE2 atom in His237 (HW1:NE2: 2.03 Å in the reactant *versus* 1.06 Å in the product) (Fig. 6 – step 3). Simultaneously, the OW oxygen attacks the substrate C1 carbon (OW:C1: 1.48 Å in the reaction product), resulting in a new tetrahedral intermediate, corresponding to the reaction coordinate used for this step. This third step has an activation Gibbs free energy of 12.5 kcal mol^{-1} and a reaction free energy of 6.1 kcal mol^{-1}. The TS was verified and presents an imaginary frequency at 558.8i cm^{-1}, corresponding to the vibration of the atoms involved in the reaction. Similarly to what was observed in step 1, the stabilization of the negative charge in O1 by the oxyanion hole residues is fundamental, as the atomic distances remain constant throughout the reaction (Met161:O1: 1.96 Å for the reactant *versus* 1.88 Å for the product; Tyr87:O1: 1.92 Å for the reactant *versus* 1.78 Å for the product). Proton HD1 remains bound to His237 (HD1: NE1: 1.03 Å in the reactant and 1.08 Å in the product), in contrast with the mechanism proposed by Feng *et al.*[42] Once again, these results show the importance of Asp206 stabilization by nearby residues, only accounted for when these are included in the QM region since in our calculations with a smaller layer (model 1), the proton was transferred in this step, as can be verified by Fig. S11.†

Finally, the last step (Fig. 6 – step 4) results in the cleavage process of the C1–OG bond (1.53 Å in the reactant *versus* 2.62 Å in the final state), releasing the final product. This was the reaction coordinate followed. The catalytic Ser160 residue that extracts hydrogen HW1 from the histidine residue (OG: HW1: 1.00 Å in the product), restabilising its initial configuration, so a new catalytic cycle can occur. The last step is characterized by the lowest activation Gibbs free energy, of 5.0 kcal mol^{-1}, and a reaction free energy of −1.7 kcal mol^{-1}. The TS of step 4 is characterized by a single imaginary frequency at 632.2i cm^{-1}.

The adduct hydrolysis occurs through two sequential steps and with a maximum activation barrier of 12.5 kcal mol^{-1}. After this stage, the enzyme is ready to start a new catalytic cycle.

Energy profile

The overall *Is*PETase mediated reaction is slightly exergonic since the final product Gibbs free energy is −4.7 kcal mol^{-1} lower than the initial reagent. The energy profile is characterized in Fig. 7 and reveals step 3 as the rate-limiting step of the entire mechanism, with a cumulative energy barrier of 12.5 kcal mol^{-1}, which closely agrees with the experimentally determined k_{cat} values for this enzyme.[17,28] Details on the energy components for this profile can be found in Tables S10–S13.†

In the mechanism proposed by Jerves *et al.*[43] studied with a larger substrate than used here, the formation of the first intermediate (steps 1 and 2 in our proposal) occurs in one step with an activation Gibbs free energy of 20.0 kcal mol^{-1}, making it the rate-limiting step of the reaction. Jerves *et al.*[43] treated the QM region with DFT, using a PBE functional and DZVP-GTH-PBE basis-set. Boneta *et al.*[41] study treated the QM region with the semiempirical AM1 methods post-corrected with the M06-2X functional and the 6-31+G(d,p) basis set. According to Boneta *et al.*,[41] that have determined a four-step mechanism with a larger substrate, the rate-limiting step corresponds to step 2 with an activation Gibbs free energy of 18.9 kcal mol^{-1}. Finally, in the mechanism advanced by Feng *et al.*,[42] (M06-2X/6-31G(d) geometry optimizations, and M06-2X/6-311G(d,p) for single point energies) steps 1 and 4 are competitive rate-limiting steps, albeit with higher energy barriers and a larger associated dispersion error determined. Moreover, this last work was studied considering a smaller QM region, where a set of important residues for the stabilization of the Asp206 residue was not included.

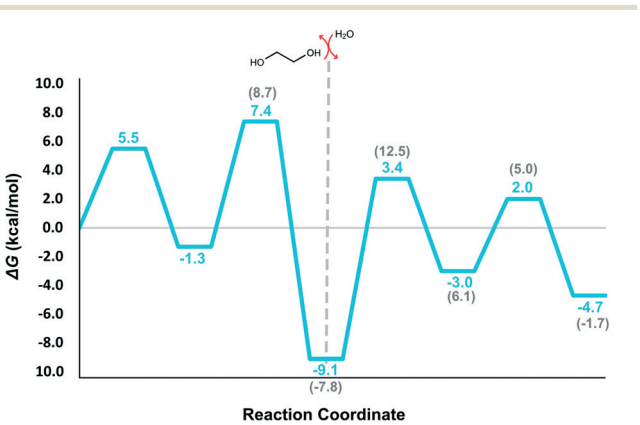

Fig. 7 Complete energy profile for the catalytic mechanism of PETase, obtained with model 3. The values placed between parentheses correspond to the activation/reaction Gibbs free energies of each step.

The comparison between the energy profiles obtained with all three models studied is available in Fig. S6,† and the details can be found in Tables S2–S5† for model 1 and Tables S6–S9† for model 2.

The impact of Trp185

As evidenced by the comparison of the energy profiles obtained for models 2 and 3 (Fig. S6†), the profiles are fairly similar, slightly stabilising all minima. However, careful analysis of the catalytic environment led us to consider the impact of Trp185 in the process and to conduct studies with an expanded model (model 3). Trp185 is conserved in several PET degrading enzymes, but in *Is*PETase assumes three different conformations, having been designated as a wobbly tryptophan.[72] The strong π–π interaction between Trp185 and the substrate is observed in all mechanism steps, and is essential for substrate fixing and position. This is further supported by experimental evidence of activity loss upon replacement of Trp185.[73]

The impact of Ser207, Ile208 and Ala209

Initially, our calculations were performed with a smaller QM region, corresponding to model 1 described in the methodology section. This model was built based on the *Is*PETase mechanism proposed by Han *et al.*[18] to include the relevant catalytic residues, the HEMT substrate and the stabilizing oxyanion hole. To investigate the nearby residues' influence on the activation and reaction energies for each step, the contributing charges for residues from the MM region at 2, 3, 4 and 5 Å of the QM region were set zero, and single-point energies for the reactant, TS, and product structures were calculated. Comparison of the re-calculated energies with the ones obtained for the initial model revealed residues Ser207, Ile208 and Ala209, and of a specific water molecule to heavily influence the activation and reaction energies, as can be observed in Fig. 8 for the first reaction step.

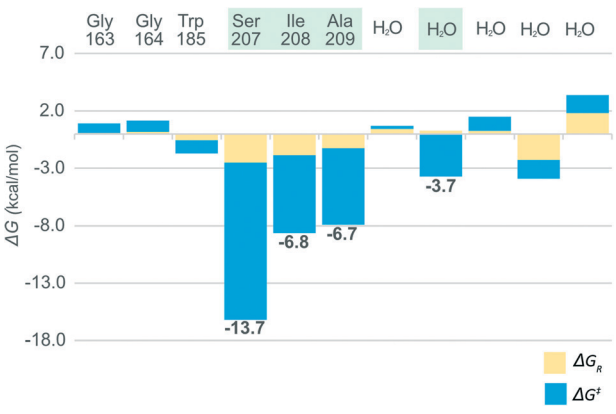

Fig. 8 Differences between the calculated single-point energies for the residues with null charges 2 Å away from the QM region residues in step 1, revealing that residues Ser207, Ile208 and Ala181 and of a specific water molecule had a large influence in the final energy.

The results for the remaining steps are included in ESI† (Fig. S7–S10). The mentioned residues were found to closely interact with catalytic Asp206 residue and provide the necessary stabilization for the shared hydrogen atom between catalytic His237 and Asp206. The essential role of Ile208 has been confirmed by mutagenesis studies with effects on activity.[18,19] Han *et al.*[18] measured the activity of I208A against PET film, resulting in a significant decrease in activity (~20% MHET release compared with WT enzyme). Similarly, when Joo *et al.*[19] performed the same mutation using BHET as a substrate, the engineered variant resulted in 46% activity when compared with WT.

The combined computational and experimental evidence justified the increase of the QM region, resulting in model 2. With this model, as described previously, hydrogen HD1 remains bound to His237, not being transferred to Asp206, due to the increased stabilization of the catalytic aspartate. In our initial studies with a smaller QM region (model 1), we observed the transference of this atom, similarly to Boneta *et al.*[41] mechanistic proposal, in which a smaller QM region was also used. Specific distances between hydrogen HD1 and His237 and Asp206 residues for all models can be found in Fig. S11.†

The particular role of Ile208

A further investigation on the role of Ile208 was conducted to rationalize the experimental observations of lower enzymatic activity upon I208A mutation. A 100 ns MD simulation of the mutated (I208A) structure was run. The results confirm that this replacement hinders the stability of the catalytic Asp206, disrupting the charge-relay system between Asp206 and His237, as evidenced by Fig. 9–11. Fig. 9 shows how the distance between the OD2 oxygen of Asp206 and the HD1 hydrogen in His237 differs in the WT structure simulation and in the mutated one. When Ile208 is replaced by an Ala residue, the distance between the two catalytic residues is much larger and varied along the simulation, disrupting the charge-relay system that allows the stabilization of the intermediate double-protonated His237 by the Asp206. Furthermore, for WT *Is*PETase, the hydrogen bond between Asp206 and His237 is kept for

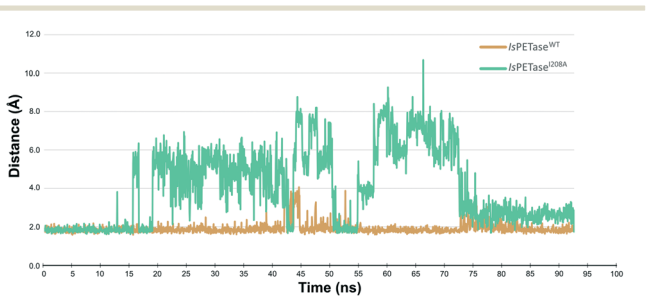

Fig. 9 Distance between atoms OD2 of Asp206 and HD1 of His237 throughout a 100 ns simulation in WT *Is*PETase (orange) and mutated *Is*PETase (green).

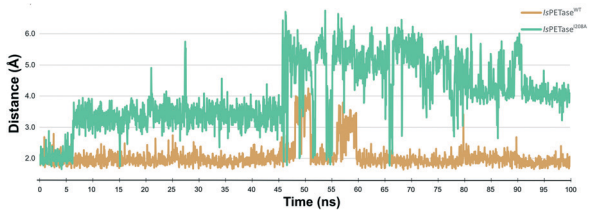

Fig. 10 Distance between Asp206 and residue Ile208 (orange) or Ala208 (green) throughout a 100 ns MD simulation comparison WT with mutated *Is*PETase, respectively.

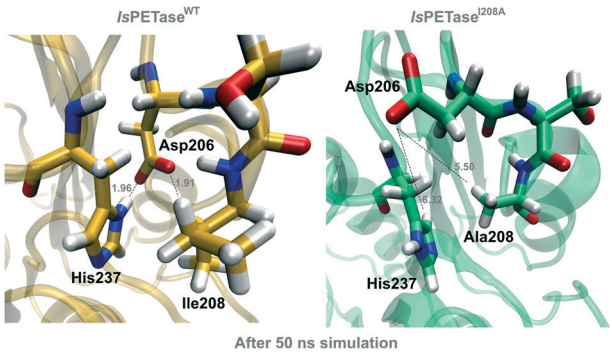

Fig. 11 Structural comparison between the distances of Asp206, His237, and Ile208 (orange) or Ala208 (green) after 50 ns of simulation in WT (orange) and mutated (green) structures.

96% of the 100 ns MD simulation, while in *Is*PETase^{I208A} this interaction only occurs 31% of the time. This can be partially explained by what is observed in Fig. 10, since the distance between Ile208 and Asp206 is much smaller and constant than the distance between mutated residue Ala208 and Asp206. The loss of this hydrogen bond destabilizes the catalytic residues. This is further evidenced by the structural shot in Fig. 11, obtained after 50 ns of simulation, in which it is evident the displacement that Asp206 suffers in the absence of Ile208. Although the mutation does not change the atoms directly involved in the interaction with the Asp206, the replacement by a smaller residue weakens this interaction. Thus, Ile208 is not only relevant for Asp206 basicity control but also affects its positioning within the active site. The lipophilicity reduction when Ile208 is replaced by an Ala increases Asp206 mobility and its tendency to be solvent exposed.

Conclusion

In this work, molecular dynamics simulations and QM/MM calculations were employed to describe the catalytic mechanism of *Is*PETase. Our calculations suggested a catalytic mechanism through four sequential steps. The first two steps lead to the elimination of the EG and the formation of an HMET-enzyme adduct. Then, two additional steps are required for the hydrolysis of the adduct and the release of the final product.

According to the computed Gibbs free energies, the third step is the rate-limiting process of the entire mechanism, requiring 12.5 kcal mol^{-1}, which closely agrees with the experimental available kinetic data for this enzyme (15.8 to 18.0 kcal mol^{-1}).[17,28]

This work has shown, for the first time, the critical role of a trio of residues in the stabilization of Asp206. According to our simulations, Ser207, Ile208, and Ala209 reduce the basic character of Asp206, precluding the HD1 proton abstraction from His237. Moreover, the presence of the Asp206 residue is crucial in the stabilization of the transient and double protonated His237, being therefore a nonparticipant essential element in the catalytic reaction. This effect seems to speed up the reaction and provides insights about the reasons behind the loss of activity when Ile208 is mutated by an Ala. Although Ile and Ala are non-polar residues, Ile208 stabilizes the Asp206 through its backbone amine group. Our results show that Ile208 mutation by a considerably smaller residue (Ala) impairs this interaction.[18,19] In fact, the lack of proper (QM) description of this interaction led to higher barriers as obtained in our calculations with model 1 and other already published works.[41,42]

The new insights provided in this work can deeply contribute to a better understanding of PETase enzymes, suggesting new ways to engineer this enzyme for better efficiency in PET degradation. Particularly, the Asp206 surrounding region could arise an exploration topic to produce more efficient biocatalysts for plastic degradation.

Author contributions

RPM has done the investigation, formal analysis, visualization, and writing of the original draft. HSF has supervised, developed the methodology, and reviewed the manuscript. SFS has conceptualized the project, supervised, acquired funding, administrated the project, and reviewed the manuscript.

Conflicts of interest

There are no conflicts to declare.

Acknowledgements

This work was supported by the Applied Molecular Biosciences Unit—UCIBIO and Associate Laboratory i4HB, which are financed by national funds from FCT (UIDP/04378/2020, UIDB/04378/2020, and LA/P/0140/2020). This work was also partially supported by the PTDC/QUI-QFI/31689/2017 project financed by FCT. SS acknowledges the grant 2020.01423.CEECIND. RM acknowledges FCT for the PhD grant 2020.09087.BD. Some of the calculations were produced with the support of INCD funded by FCT and FEDER under the projects 01/SAICT/2016 number 022153, and projects CPCA/A00/7140/2020, and CPCA/A00/7145/2020.

References

1 A. Amobonye, P. Bhagwat, S. Singh and S. Pillai, *Sci. Total Environ.*, 2021, **759**, 143536.
2 R. Geyer, J. R. Jambeck and K. L. Law, *Sci. Adv.*, 2017, **3**(7), DOI: **10.1126/sciadv.1700782**.
3 P. Li, X. Wang, M. Su, X. Zou, L. Duan and H. Zhang, *Bull. Environ. Contam. Toxicol.*, 2021, **107**(4), 577–584.
4 J. Hopewell, R. Dvorak and E. Kosior, *Philos. Trans. R. Soc., B*, 2009, **364**, 2115–2126.
5 A. L. Andrady and M. A. Neal, *Philos. Trans. R. Soc., B*, 2009, **364**, 1977–1984.
6 H. T. H. Nguyen, P. Qi, M. Rostagno, A. Feteha and S. A. Miller, *J. Mater. Chem. A*, 2018, **6**, 9298–9331.
7 I. Taniguchi, S. Yoshida, K. Hiraga, K. Miyamoto, Y. Kimura and K. Oda, *ACS Catal.*, 2019, **9**, 4089–4105.
8 A. Saravanan, P. S. Kumar, D.-V. N. Vo, S. Jeevanantham, S. Karishma and P. R. Yaashikaa, *J. Hazard. Mater.*, 2021, **419**, DOI: **10.1016/j.jhazmat.2021.126451**.
9 F. Kawai, T. Kawabata and M. Oda, *ACS Sustainable Chem. Eng.*, 2020, **8**, 8894–8908.
10 R.-J. Müller, H. Schrader, J. Profe, K. Dresler and W.-D. Deckwer, *Macromol. Rapid Commun.*, 2005, **26**, 1400–1405.
11 F. Kawai, M. Oda, T. Tamashiro, T. Waku, N. Tanaka, M. Yamamoto, H. Mizushima, T. Miyakawa and M. Tanokura, *Appl. Microbiol. Biotechnol.*, 2014, **98**, 10053–10064.
12 S. Sulaiman, D.-J. You, E. Kanaya, Y. Koga and S. Kanaya, *Biochemistry*, 2014, **53**, 1858–1869.
13 E. Herrero Acero, D. Ribitsch, G. Steinkellner, K. Gruber, K. Greimel, I. Eiteljoerg, E. Trotscha, R. Wei, W. Zimmermann, M. Zinn, A. Cavaco-Paulo, G. Freddi, H. Schwab and G. Guebitz, *Macromolecules*, 2011, **44**, 4632–4640.
14 M. Dimarogona, E. Nikolaivits, M. Kanelli, P. Christakopoulos, M. Sandgren and E. Topakas, *Biochim. Biophys. Acta*, 2015, **1850**, 2308–2317.
15 L. Su, R. Hong, D. Kong and J. Wu, *Int. J. Biol. Macromol.*, 2020, **162**, 1752–1759.
16 S. Heumann, A. Eberl, H. Pobeheim, S. Liebminger, G. Fischer-Colbrie, E. Almansa, A. Cavaco-Paulo and G. M. Gübitz, *J. Biochem. Biophys. Methods*, 2006, **69**, 89–99.
17 S. Yoshida, K. Hiraga, T. Takehana, I. Taniguchi, H. Yamaji, Y. Maeda, K. Toyohara, K. Miyamoto, Y. Kimura and K. Oda, *Science*, 2016, **351**, 1196–1199.
18 X. Han, W. Liu, J.-W. Huang, J. Ma, Y. Zheng, T.-P. Ko, L. Xu, Y.-S. Cheng, C.-C. Chen and R.-T. Guo, *Nat. Commun.*, 2017, **8**(1), DOI: **10.1038/s41467-017-02255-z**.
19 S. Joo, I. J. Cho, H. Seo, H. F. Son, H.-Y. Sagong, T. J. Shin, S. Y. Choi, S. Y. Lee and K.-J. Kim, *Nat. Commun.*, 2018, **9**(1), DOI: **10.1038/s41467-018-02881-1**.
20 T. Fecker, P. Galaz-Davison, F. Engelberger, Y. Narui, M. Sotomayor, L. P. Parra and C. A. Ramírez-Sarmiento, *Biophys. J.*, 2018, **114**, 1302–1312.
21 H. P. Austin, M. D. Allen, B. S. Donohoe, N. A. Rorrer, F. L. Kearns, R. L. Silveira, B. C. Pollard, G. Dominick, R. Duman, K. E. Omari, V. Mykhaylyk, A. Wagner, W. E. Michener, A. Amore, M. S. Skaf, M. F. Crowley, A. W. Thorne, C. W. Johnson, H. Lee Woodcock, J. E. McGeehan and G. T. Beckham, *Proc. Natl. Acad. Sci. U. S. A.*, 2018, **115**, E4350–E4357.
22 B. Liu, L. He, L. Wang, T. Li, C. Li, H. Liu, Y. Luo and R. Bao, *ChemBioChem*, 2018, **19**, 1471–1475.
23 C. Liu, C. Shi, S. Zhu, R. Wei and C.-C. Yin, *Biochem. Biophys. Res. Commun.*, 2019, **508**, 289–294.
24 G. J. Palm, L. Reisky, D. Böttcher, H. Müller, E. A. P. Michels, M. C. Walczak, L. Berndt, M. S. Weiss, U. T. Bornscheuer and G. Weber, *Nat. Commun.*, 2019, **10**(1), DOI: **10.1038/s41467-019-09326-3**.
25 H. F. Son, I. J. Cho, S. Joo, H. Seo, H.-Y. Sagong, S. Y. Choi, S. Y. Lee and K.-J. Kim, *ACS Catal.*, 2019, **9**, 3519–3526.
26 H. F. Son, S. Joo, H. Seo, H.-Y. Sagong, S. H. Lee, H. Hong and K.-J. Kim, *Enzyme Microb. Technol.*, 2020, **141**, DOI: **10.1016/j.enzmictec.2020.109656**.
27 R. P. Magalhães, J. M. Cunha and S. F. Sousa, *Int. J. Mol. Sci.*, 2021, 22.
28 Y. Ma, M. Yao, B. Li, M. Ding, B. He, S. Chen, X. Zhou and Y. Yuan, *Engineering*, 2018, **4**, 888–893.
29 H. S. Fernandes, S. F. Sousa and N. M. F. S. A. Cerqueira, *Mol. Diversity*, 2021, DOI: **10.1007/s11030-021-10259-7**.
30 K. Świderek and V. Moliner, *Chem. Sci.*, 2020, **11**, 10626–10630.
31 M. Dixit, M. Weitman, J. Gao and D. T. Major, *ACS Catal.*, 2017, **7**, 812–818.
32 P. Ferreira, P. A. Fernandes and M. J. Ramos, *Chem. – Eur. J.*, 2021, **27**, 13998–14006.
33 F. Planas, M. J. McLeish and F. Himo, *ACS Catal.*, 2021, **11**, 12355–12366.
34 A. F. Pina, S. F. Sousa and N. M. F. S. A. Cerqueira, *ChemBioChem*, 2021, DOI: **10.1002/cbic.202100555**.
35 S. Sudhakara, C. Ramakrishnan, M. M. Gromiha and A. Chadha, *Catal. Sci. Technol.*, 2020, **10**, 5925–5934.
36 E. F. Oliveira, N. M. F. S. A. Cerqueira, M. J. Ramos and P. A. Fernandes, *Catal. Sci. Technol.*, 2016, **6**, 7172–7185.
37 M. H. Weiland, in *Mechanistic Enzymology: Bridging Structure and Function*, American Chemical Society, 2020, vol. 1357, pp. 161–174 SE–8.
38 B. C. Knott, E. Erickson, M. D. Allen, J. E. Gado, R. Graham, F. L. Kearns, I. Pardo, E. Topuzlu, J. J. Anderson, H. P. Austin, G. Dominick, C. W. Johnson, N. A. Rorrer, C. J. Szostkiewicz, V. Copié, C. M. Payne, H. L. Woodcock, B. S. Donohoe, G. T. Beckham and J. E. McGeehan, *Proc. Natl. Acad. Sci. U. S. A.*, 2020, **117**, 25476–25485.
39 A. Papadopoulou, K. Hecht and R. Buller, *Chimia*, 2019, **73**, 743–749.
40 R. Wei, C. Song, D. Gräsing, T. Schneider, P. Bielytskyi, D. Böttcher, J. Matysik, U. T. Bornscheuer and W. Zimmermann, *Nat. Commun.*, 2019, **10**, 5581.
41 S. Boneta, K. Arafet and V. Moliner, *J. Chem. Inf. Model.*, 2021, **61**, 3041–3051.
42 S. Feng, Y. Yue, M. Zheng, Y. Li, Q. Zhang and W. Wang, *ACS Sustainable Chem. Eng.*, 2021, **9**, 9823–9832.
43 C. Jerves, R. P. P. Neves, M. J. Ramos, S. da Silva and P. A. Fernandes, *ACS Catal.*, 2021, **11**, 11626–11638.

44 H. M. Berman, J. Westbrook, Z. Feng, G. Gilliland, T. N. Bhat, H. Weissig, I. N. Shindyalov and P. E. Bourne, *Nucleic Acids Res.*, 2000, **28**, 235–242.

45 W. L. DeLano, The PyMOL Molecular Graphics System, **https://www.pymol.org**.

46 D. A. Case, T. E. Cheatham III, T. Darden, H. Gohlke, R. Luo, K. M. Merz Jr., A. Onufriev, C. Simmerling, B. Wang and R. J. Woods, *J. Comput. Chem.*, 2005, **26**, 1668–1688.

47 G. Martínez-Rosell, T. Giorgino and G. De Fabritiis, *J. Chem. Inf. Model.*, 2017, **57**, 1511–1516.

48 M. J. Frisch, G. W. Trucks, H. B. Schlegel, G. E. Scuseria, M. A. Robb, J. R. Cheeseman, G. Scalmani, V. Barone, G. A. Petersson, H. Nakatsuji, X. Li, M. Caricato, A. V. Marenich, J. Bloino, B. G. Janesko, R. Gomperts, B. Mennucci, H. P. Hratchian, J. V. Ortiz, A. F. Izmaylov, J. L. Sonnenberg, D. Williams-Young, F. Ding, F. Lipparini, F. Egidi, J. Goings, B. Peng, A. Petrone, T. Henderson, D. Ranasinghe, V. G. Zakrzewski, J. Gao, N. Rega, G. Zheng, W. Liang, M. Hada, M. Ehara, K. Toyota, R. Fukuda, J. Hasegawa, M. Ishida, T. Nakajima, Y. Honda, O. Kitao, H. Nakai, T. Vreven, K. Throssell, J. A. Montgomery Jr., J. E. Peralta, F. Ogliaro, M. J. Bearpark, J. J. Heyd, E. N. Brothers, K. N. Kudin, V. N. Staroverov, T. A. Keith, R. Kobayashi, J. Normand, K. Raghavachari, A. P. Rendell, J. C. Burant, S. S. Iyengar, J. Tomasi, M. Cossi, J. M. Millam, M. Klene, C. Adamo, R. Cammi, J. W. Ochterski, R. L. Martin, K. Morokuma, O. Farkas, J. B. Foresman and D. J. Fox, *Gaussian 16, Revision C.01*, Gaussian, Inc., Wallin, 2016.

49 J. A. Maier, C. Martinez, K. Kasavajhala, L. Wickstrom, K. E. Hauser and C. Simmerling, *J. Chem. Theory Comput.*, 2015, **11**, 3696–3713.

50 D. J. Price and C. L. Brooks III, *J. Chem. Phys.*, 2004, **121**, 10096–10103.

51 W. L. Jorgensen, J. Chandrasekhar, J. D. Madura, R. W. Impey and M. L. Klein, *J. Chem. Phys.*, 1983, **79**, 926–935.

52 J.-P. Ryckaert, G. Ciccotti and H. J. C. Berendsen, *J. Comput. Phys.*, 1977, **23**, 327–341.

53 D. R. Roe and T. E. Cheatham, *J. Chem. Theory Comput.*, 2013, **9**, 3084–3095.

54 W. Humphrey, A. Dalke and K. Schulten, *J. Mol. Graphics*, 1996, **14**, 33–38.

55 H. S. Fernandes, M. J. Ramos and N. M. F. S. A. Cerqueira, *J. Comput. Chem.*, 2018, **39**, 1344–1353.

56 H. S. Fernandes, S. F. Sousa and N. M. F. S. A. Cerqueira, *J. Chem. Inf. Model.*, 2019, **59**, 4519–4523.

57 S. Dapprich, I. Komáromi, K. S. Byun, K. Morokuma and M. J. Frisch, *J. Mol. Struct.: THEOCHEM*, 1999, **461–462**, 1–21.

58 A. D. Becke, *Phys. Rev. A: At., Mol., Opt. Phys.*, 1988, **38**, 3098–3100.

59 C. Lee, W. Yang and R. G. Parr, *Phys. Rev. B: Condens. Matter Mater. Phys.*, 1988, **37**, 785–789.

60 P. J. Stephens, F. J. Devlin, C. F. Chabalowski and M. J. Frisch, *J. Phys. Chem.*, 1994, **98**, 11623–11627.

61 K. Fukui, *Acc. Chem. Res.*, 1981, **14**, 363–368.

62 Y. Guo, C. Riplinger, U. Becker, D. G. Liakos, Y. Minenkov, L. Cavallo and F. Neese, *J. Chem. Phys.*, 2018, **148**(1), DOI: **10.1063/1.5011798**.

63 F. Neese, *WIREs Comput. Mol. Sci.*, 2012, **2**, 73–78.

64 P. Paiva, S. F. Sousa, P. A. Fernandes and M. João Ramos, *ChemCatChem*, 2019, **11**, 3853–3864.

65 C. S. S. Teixeira, M. J. Ramos, S. F. Sousa and N. M. F. S. A. Cerqueira, *ChemCatChem*, 2020, **12**, 227–237.

66 J. P. M. Sousa, R. P. P. Neves, S. F. Sousa, M. J. Ramos and P. A. Fernandes, *ACS Catal.*, 2020, **10**, 9545–9554.

67 P. M. G. Ribeiro, H. S. Fernandes, L. B. Maia, S. F. Sousa, J. J. G. Moura and N. M. F. S. A. Cerqueira, *Inorg. Chem. Front.*, 2021, **8**, 405–416.

68 C. S. Silva Teixeira, S. F. Sousa and N. M. F. S. A. Cerqueira, *ChemPhysChem*, 2021, **22**, 796–804.

69 P. Mihaljević-Jurič and S. F. Sousa, *Process*, 2021, 9.

70 M. J. Frisch, **https://www.gaussian.com/**.

71 R. P. Magalhães, H. S. Fernandes and S. F. Sousa, *Isr. J. Chem.*, 2020, **60**, 655–666.

72 X. Han, W. Liu, J.-W. Huang, J. Ma, Y. Zheng, T.-P. Ko, L. Xu, Y.-S. Cheng, C.-C. Chen and R.-T. Guo, *Nat. Commun.*, 2017, **8**, 2106.

73 S. Joo, I. J. Cho, H. Seo, H. F. Son, H.-Y. Sagong, T. J. Shin, S. Y. Choi, S. Y. Lee and K.-J. Kim, *Nat. Commun.*, 2018, **9**, 382.